Astron. Astrophys. 338, 329–339 (1998)

ASTRONOMY
AND
ASTROPHYSICS

Numerical 3D simulations of buoyant magnetic flux tubes

S.B.F. Dorch and Å. Nordlund

The Niels Bohr Institute for Astronomy, Physics and Geophysics, Juliane Maries Vej 30, DK-2100 Copenhagen Ø, Denmark
(e-mail: dorch@astro.ku.dk; aake@astro.ku.dk)

Received 25 July 1996 / Accepted 1 July 1998

Abstract. We have examined instabilities of non-thin buoyant magnetic flux tubes ascending through a solar convection zone model using numerical 3D MHD experiments. The experiments show that the fate of the flux tubes is entirely dependent on the internal topology of the magnetic field lines in the flux tube; if the initial topology is too simple the tube is quickly disrupted by a Rayleigh-Taylor like instability. The disruption is prevented or delayed if the field has a component that makes the topology non-trivial. Even a weak random or twisting component, an order of magnitude weaker than the longitudinal magnetic field, is sufficient to let the tube ascend as a more or less coherent structure. These 3D results may resolve the apparent contradiction between the success of experiments using the thin flux tube approximation to study the buoyant rise of magnetic flux tubes, and the rapid break-up of flux tubes found in 2D experiments.

Key words: Sun: activity – sunspots – Sun: magnetic fields instabilities – MHD

1. Introduction

A solar active region is initiated as a lot of small scale magnetic flux emerges on the solar surface. Gradually more magnetic flux appears in the emerging magnetic flux region (EFR) that grows in size, resulting in a large bipolar magnetic region where eventually pores and sunspots form. After the formation of the sunspots, magnetic flux continues to appear in the EFR (cf. Gaizauskas 1993). The observational evidence thus indicates that the magnetic field out of which the active region is formed exists in the form of a lot of small scale structures in the subphotosphere and top convection zone.

The current belief is that active regions are formed when magnetic flux loops from the interior of the Sun penetrate the photosphere. The emerging magnetic fields are thought to have their origin in a toroidal flux system that resides in the undershoot layer between the convective envelope and the stably stratified radiative interior of the Sun. The cyclic process responsible for the formation of the toroidal flux system is probably, in broad terms, a combined effect of the solar differential rotation, a shear in the undershoot layer and turbulent convection. A likely scenario is the dynamic Babcock-Leighton dynamo (cf. Parker 1955; Babcock 1961; Leighton 1964, 1969; Wang & Sheeley 1991; Wang et al. 1991; Sheeley 1992).

One aspect of the dynamo is, apparently, the formation of a strong toroidal magnetic flux system in the undershoot layer, with magnetic energies of the order of a hundred times the values that result from equipartition with the kinetic energy (Choudhuri & Gilman 1987; Choudhuri 1989; Moreno-Insertis et al. 1992). When this flux system is subjected to instabilities fragments of it erupt and form the observed magnetic activity cycle.

Recent models of rising magnetic flux tubes show results that are in agreement with the observed tilt angles and emergence latitudes for active regions and sunspots (D'Silva & Choudhuri 1993; Fan et al. 1993; Fan et al. 1994; Caligari et al. 1995). One can even understand the scattering in the tilt angles as a consequence of convection zone turbulence (Longcope & Fisher 1996). Against this background it may seem that the behavior of buoyant magnetic flux tubes in the convection zone is well understood.

There are, however, several problems. Firstly, these numerical experiments so far have assumed that the magnetic field ascends in the form of nice, coherent (even closed) flux tubes that remain intact as they ascend. Secondly, most of the experiments have used the 'thin flux tube approximation' (cf. Spruit 1981; Moreno-Insertis 1986; Choudhuri 1989) and the numerical experiments have therefore been stopped at, or near, the point where this assumption breaks down; around 10-20 Mm below the photosphere. However, all observations of EFRs show that an EFR does not consist of a nice coherent flux tube but rather is made up of a lot of smaller flux tubes that only later merge to form pores and sunspots.

How can it be then that the numerical experiments agree so well with the observations? We must conclude on the one hand, that the flux tubes are apparently able to maintain their integrity throughout most of the convection zone — if they were not, then eg. the ratios of buoyancy to drag assumed in the calculations would be grossly in error (but see Choudhuri & D'Silva 1990; D'Silva & Choudhuri 1991; Choudhuri 1992; D'Silva 1993 for an alternative scenario). On the other hand, once the tubes do get close enough to the surface they obviously break up into smaller flux tubes.

Send offprint requests to: S.B.F. Dorch

There are at least two mechanisms that may be responsible for the break-up of flux tubes near the solar surface. The first has to do with the range of validity of the thin flux tube approximation. As a flux tube ascends, the ratios of its size to the local pressure and density scale heights increase, both because its size increases and because the scale heights decrease. A flux tube that is larger than the local pressure and density scale heights induces a strongly anisotropic external velocity field, and horizontal pressure fluctuations that are large compared to the average pressure. It seems plausible that such a flux tube would be subject to instabilities that split it into fragments whose size are comparable to the scale heights.

The second mechanism that may cause break-up of flux tubes appears already within the framework of the thin flux tube approximation. As a toroidal flux tube rises and expands adiabatically it may at some point, depending on its initial field strength, encounter a layer where the internal gas pressure equals the external pressure. At this height a flux tube 'explosion' may set in (cf. Moreno-Insertis et al. 1995) if hydrostatic equilibrium is obtained along field lines. If the initial field strength is large enough this layer will be close to the photosphere, and if the total magnetic flux is large the ascent may be sufficiently fast for hydrostatic equilibrium along the tube not to be obtained. However, for weak and / or small flux tubes this effect may set in before the previously mentioned mechanism.

In any case, after the flux tubes have emerged, and the legs anchored deep in the convection zone have had time to establish hydrostatic equilibrium, the existence of a layer where the internal pressure equals the external pressure would imply that there was no net restraining force. Fan et al. (1994) proposed the name 'dynamic disconnection' for this situation (though in their case it may be strongly influenced by their initial configuration). The mechanism provides a possible explanation for the disconnection of surface magnetic fields from the global toroidal flux system to let them drift more or less freely on the solar surface as observed.

Thus, a reasonably consistent picture emerges; fragments of the toroidal flux system become buoyantly unstable at field strengths of around 10^5 G, ascend to the surface, and emerge after breaking into smaller fragments just beneath the surface. However, there is a fundamental difficulty with this picture: As has been shown by Schüssler (1979), a Rayleigh-Taylor like instability threatens to split rising flux tubes long before they even come close to the surface. This is an important problem, since the consequences would bring the nice thin flux tube results into question. Recently, Longcope et al. (1996) have reiterated the problem, concluding that "an isolated horizontal tube of flux can rise only a few of its own radii before fragmenting". Emonet & Moreno-Insertis (1996b), Emonet & Moreno-Insertis (1997) and Emonet & Moreno-Insertis (1998) find similar results, but in addition show that the splitting instability can be inhibited by introducing a uniform twist of the flux tubes, if the tangent of the maximum pitch angle exceeds $(\frac{R}{H_P})^{\frac{1}{2}}$, where R is the tube radius and H_P the pressure scale height. Earlier 2D results on the splitting instability are by Tsinganos (1980), Cattaneo & Hughes (1988), Cattaneo et al. (1990), Matthews et al. (1995), Emonet & Moreno-Insertis (1996a) and Moreno-Insertis (1997). In the subsequent sections we report on numerical experiments that demonstrate that this difficulty is likely to be an artifact of using oversimplified models. Sect. 2 discusses the model we adopt. Results and discussions are presented in Sect. 3, and the conclusions are drawn in Sect. 5.

2. The model

The objective of these numerical experiments is to study instabilities in buoyant magnetic flux tubes. For this purpose we need to solve the MHD equations in a stratified medium, bounded below by a stable layer. We use periodic boundary conditions in the horizontal directions, and a top boundary that is a 'virtual boundary'; i.e., it is a mathematical boundary whose influence on the solution we attempt to minimize.

2.1. The equations

The equations that we use are the MHD equations in the absence of rotation, written in conservative form:

$$\frac{\partial \rho}{\partial t} + \nabla \cdot \rho \mathbf{u} = 0, \tag{1}$$

$$\frac{\partial \rho \mathbf{u}}{\partial t} = -\nabla \cdot (\rho \mathbf{u}\mathbf{u} - \tau) - \nabla P + \mathbf{j} \times \mathbf{B} + \rho \mathbf{g}, \tag{2}$$

$$\frac{\partial \mathbf{B}}{\partial t} = -\nabla \times \mathbf{E}, \tag{3}$$

$$\mu_0 \mathbf{j} = \nabla \times \mathbf{B}, \tag{4}$$

$$\mathbf{E} = \eta \mathbf{j} - \mathbf{u} \times \mathbf{B}, \tag{5}$$

$$\frac{\partial e}{\partial t} = -\nabla \cdot (e\mathbf{u}) - P \nabla \cdot \mathbf{u} + Q_{\rm rad} + Q_{\rm visc} + Q_{\rm Joule}, \tag{6}$$

where ρ is the mass density, $\mathbf{u}$ the velocity, τ the viscous stress tensor, P the pressure, $\mathbf{B}$ the magnetic field, $\mathbf{j}$ the electric current, $\mathbf{g}$ the gravity, $\mathbf{E}$ the electric field, η the magnetic diffusivity, e the internal energy per unit volume and the Q's are the radiative energy transfer and the viscous and Joule dissipation respectively.

2.2. Dimensions and boundary conditions

Geometrically, the MHD model consists of a box containing $n_x \times n_y \times n_z$ grid points. The physical dimensions corresponding to the model are $L_x = (n_x - 1)\Delta x$, $L_y = n_y \Delta y$ and $L_z = n_z \Delta z$, where Δx, Δy and Δz are the distances between grid points. For reasons of computational efficiency (on a CM-200), we use x as the vertical dimension. The y-axis corresponds to the azimuthal (toroidal) direction in a spherical geometry, and the z-axis corresponds to the polar direction.

Using the numerical scheme of Nordlund & Galsgaard (1997), a solution to Eqs. (1) –

(6) is obtained in the form of snapshots of ρ, ρu_x, ρu_y, ρu_z, e, B_x, B_y and B_z on a staggered mesh; the density and internal energy are centered inside a mesh cube, the momenta and magnetic field components are centered on the cube faces. The time stepping is performed by a third order predictor-corrector method (Hyman 1979) and the number of time steps between each snapshot is typically 500, corresponding to about 0.33 sound travel times $\tau_s = L_x/\max(c_s)$ for $n_x = 512$.

In order to implement the boundary conditions in the vertical direction, we place *ghost zones* in the index ranges $x \in [1 : 4] \wedge [n_x - 4 : n_x]$. The y- and z-directions are taken to be periodic.

In order to allow the magnetic field to ascend through the upper boundary, the velocity in the ghost zones that determines the electric field, and thus the partial time derivatives of the magnetic field, is taken to be an extrapolation of the velocity $\mathbf{u}$ inside the box so that $\mathbf{E} = -\mathbf{u} \times \mathbf{B}$. In general, such an open boundary condition is unstable, but in the case of a stratified model an auxiliary boundary condition on the density can enforce stability; we assume that

$$\frac{\partial \rho}{\partial t} = -(1+\epsilon) u_x \frac{\partial \rho}{\partial x} \tag{7}$$

at the upper boundary, where ϵ is a small, positive quantity (we use $\epsilon = 0.1$). This corresponds to assuming that the density at the upper boundary varies in the same sense as (but slightly faster than) for vanishing Lagrangian variation. Thus, the Lagrangian variation (following the motion) is such as to increase the density when fluid is going out and to decrease the density when fluid is coming in. This is sufficient to prevent run-away caused by the boundary extrapolation of the velocity.

2.3. Initial conditions

To make sure that the background convection zone model is in hydrostatic equilibrium we first find an entropy profile that describes the convection zone and the undershoot layer. We adopt the entropy profile of Fan et al. (1994) as the starting point. Going outwards through the solar interior the entropy increases linearly because we adopt a constant subadiabatic stratification until the bottom of the convection zone is reached. From there on the entropy decreases according to the model by Spruit (1974). At first the decrease is extremely slow, so that the entropy is almost constant, but in the top portion the conditions become noticeably superadiabatic.

Given the entropy profile, it is possible to obtain the hydrostatic pressure and density by a simple one dimensional iteration scheme.

We consider three initial conditions for the magnetic flux tube. In all three cases the field strength is given by

$$\mathbf{B}(x,\ y,\ z) = \left(-\frac{\partial A_y}{\partial z},\ B_y,\ \frac{\partial A_y}{\partial x} \right), \tag{8}$$

where B_y does not depend on y (which is taken along the flux tube axis) so that the magnetic field is divergence free. In the first case (henceforth IC1), $A_y = 0$ and thus the magnetic field strength is almost constant inside the flux tube; the field strength is an exponential of the radial distance from the center of the tube to the 7^{th} power. In the second case (IC2), A_y is also zero, while the magnetic field profile across the tube is Gaussian. In the third case (IC3), the magnetic field is similar to that in IC1, but has an additional weak transversal contribution given by

$$A_y = A_0 \times f_C(x,y,z) \times G(\mathbf{r})^4, \tag{9}$$

where G is a Gaussian, and f_C is composed of a sum of sine and cosine functions with amplitudes sampled from a random number generator, and raised to low powers. The exact form of this random part is not significant, but it should be noted that the average of A_y across the tube does not vanish exactly, and hence the resulting magnetic field has both a random and a systematic transversal component.

The transverse component of the field $B_\phi = \sqrt{B_x^2 + B_z^2}$ is determined by the parallel component of the vector potential, $\mathbf{A} = (0, A_y, 0)$, and is an order of magnitude smaller than the parallel component, so that the maximum pitch angle $\tan \Psi = B_\phi / B_y$ of the field lines is of the order of 10 degrees.

In order to skip the initial slow evolution that a purely horizontal flux tube located in the undershoot layer would have experienced after an initial perturbation, we assume that the top part of the flux tube is already in the convection zone. In some of the experiments the flux tube has a significant curvature and is located rather high up in the convection zone. The initial buoyant rise of thin flux tubes is well understood and, as discussed in the introduction, this study concentrates on the possible breakdown of flux tubes once they are in the convection zone.

We set the initial entropy of the tubes equal to the entropy at the bottom of the convection zone ($S_\mathrm{i} = 0$), and hence the tubes are not in mechanical equilibrium, because this would imply $S_\mathrm{i} < S_\mathrm{e}$.

Typical values of the magnetic field strength correspond to a plasma beta β of the order of 10. Adopting these values, that are unrealistic for the Sun, serves the purpose of reducing the cost of 3D experiments to acceptable values. Since we are solving the compressible MHD equations, the time step is limited to a fraction of the sound travel time between grid points. Typical time steps are of the order of 1 s. Buoyancy increases as the square of the magnetic field and, since the drag force is quadratic in the velocity, the final ascent velocity is proportional to B. With a magnetic field a factor of 10–100 larger than the solar field, the time scales that result from our simulations are correspondingly about 10–100 times smaller than the time scales in the Sun.

In order to hold on to the lower parts of the flux tube in the cases with an undulatory flux tube, we increase the subadiabaticity in proportion to the increased buoyancy.

The flow patterns that develop are driven by the buoyancy, and hence the speed of evolution of the instabilities scales with the buoyant rise time. To check that exaggerating the magnetic field strength only changes the time scale, but leaves the overall pattern of motion of the ascending flux structure unchanged (at least as long as the flow speeds remain substantially sub-sonic), we also ran a few experiments with a lower fields strength but the same initial field pattern.

In more realistic models, as well as in the Sun, the evolution of the buoyant flux tubes would be influenced by the turbulent convection. That influence would be stronger for weaker fields, and hence would be underestimated at the field strengths that we adopt here. But since we do not include turbulent convection in our models, we are free to modify the evolutionary time scales, by scaling the magnetic field amplitudes. More detailed models, presently out of reach because of prohibitive computational demands, should both include the turbulent convection and use realistic magnetic field strengths.

The initial conditions for the magnetic field were chosen to study the dependence on the detailed distribution of the magnetic field in the flux tube cross sections. The initial condition IC1 corresponds to a thin flux tube that has been resolved, but still has an almost constant field across the tube. In the case IC2 the magnetic field strength varies significantly across the tube, but the field lines are still parallel. In the last case (IC3), the magnetic fieldlines are interwoven, and are no longer parallel.

3. Results and discussion

We conducted a number of experiments with the model described in the previous section. Both 3D and 2D experiments of various dimensions and sizes and with various initial and boundary conditions were performed (cf. Table 1). We do not discuss the detailed results of all the experiments, but restrict ourselves to the three experiments numbered E9, E16, and E17. In E9 the tube is initially curved and the footpoints are anchored in the stable lower layer. In E16 and E17 the tubes are straight and located in the upper layer. The remaining experiments are consistent with the ones that are discussed.

3.1. The magnetic field strength

The magnetic field strength B decreases as the flux tube ascends into layers of decreasing total pressure and hence expands. The right hand side of the Walén equation (which is valid for $\eta = 0$)

$$\frac{D}{Dt}\left(\frac{B}{\rho}\right) = \left(\frac{\mathbf{B}}{\rho}\cdot\nabla\right)\mathbf{u}, \tag{10}$$

is zero if there are no motions along the tube; i.e. the ratio of B to ρ must remain constant unless the tube is stretched.

Numerical diffusion becomes important if the flux tube is only a few mesh points, or if a larger flux tube develops structure on such small scales. As we shall see this does indeed happen, and numerical diffusion then decreases the magnetic field strength by diffusing the flux, as the tube attempts to develop unresolved structures.

3.2. Initial flux tube disruption

In most of the experiments cross sections through the flux tubes evolve into a mushroom shape, consistent with the results of Schüssler (1979). Over time the structure eventually breaks up into two separate, counter-rotating flux tubes.

Fig. 1 shows the result of experiment E9 (initial condition IC2) in four snapshots. As the flux tube rises, the central part of the flux tube (in the (z, x)-plane) moves upward faster than the rest of the tube. The slow parts of the tube begin to rotate as the flux structure continues to rise, though now at a slower pace; this creates the shape that looks like a slice through a mushroom.

Qualitatively, the behavior of the flux structure as it rises because of buoyancy is similar to the behavior of two fluids subject to the Rayleigh-Taylor instability (cf. Schüssler 1979); the plasma in the tube is lighter than the plasma outside, as in the case of the Rayleigh-Taylor instability (henceforth 'R-T instability').

If the initial flux tube has a magnetic field with a maximum at the center and significantly lower field strengths away from the center, such as the Gaussian profile of IC2, the buoyancy also has a peak in the center of the tube. This means that as the tube starts rising due to buoyancy, the central part attains a higher speed than the outer parts of the tube, thus creating the rotation associated with the mushroom-structure.

A similar thing also happens in the case of an initial flux tube with a constant field across the tube (IC1), but the reason is somewhat different. In this case, the interior of the flux tube has nearly the same field strength and hence is nearly uniformly buoyant. All points in the interior of the tube thus obtain practically the same amount of initial acceleration by buoyancy. However, in addition to buoyancy, there are also pressure forces associated with the motion of the tube through an external plasma.

The situation is similar to that of a rigid, cylindrical pipe, moving upwards through a fluid at rest. Fluid in front of the pipe is pushed aside by an over-pressure in front and is pulled back by an under-pressure behind. There is thus a pressure difference between the front and rear, and a corresponding (Stokes) drag force.

In a flux tube, with no rigidity, the interior (magnetic and gas) pressure must match the external pressure, as part of a smooth overall pattern. The resulting motion pattern is also smooth with a velocity maximum at the center. Hence the central parts of the tube obtain the largest ascent velocities also in this case, which initiates a development qualitatively similar to the one discussed earlier.

Thus, there are two separate reasons that both lead to similar behavior; 1) an uneven distribution of buoyancy inside the flux tubes and 2) the effects of the pressure perturbation.

In addition to setting the left and right parts spinning in opposite directions, the motion pattern also squeezes the top part of tube in the vertical direction, and stretches it out in the horizontal direction. The result is to create a mushroom-shaped structure with two oppositely spinning vortices connected by a rapidly thinning sheet.

The flow at the center of the connecting sheet is a stagnation point flow, which implies exponential thinning of the sheet. Thus, for any finite numerical resolution the connecting sheet soon becomes thinner that can be resolved by the numerical grid, and the connection between the two spinning vortices is eventually lost.

When magnetic diffusion becomes significant, the quantity B/ρ is no longer conserved following the motion; i.e., small scale details in the magnetic field become washed out. A higher

Table 1. Parameters for the models, listed by experiment number. The initial conditions IC1, IC2 and IC3 are defined in Sect. 2.3

Experiment	Dimensions	L_x/H_P	L_y/H_P	L_z/H_P	Initial cond.
1	$96 \times 128 \times 96$	3.2	27	27	IC2
2	$96 \times 128 \times 96$	9.4	5.4	5.4	IC2
3	$96 \times 128 \times 96$	3.2	27	6.7	IC2
4	$96 \times 128 \times 96$	3.4	16.2	1.5	IC2
5	$96 \times 128 \times 96$	3.4	16.2	1.5	IC2
6	$96 \times 128 \times 96$	3.4	16.2	1.5	IC2
7	$256 \times 256 \times 1$	3.4	16.2	0	IC2
8	$96 \times 128 \times 96$	2.7	16.2	3	IC2
9	$96 \times 128 \times 96$	2.7	16.2	3	IC2
10	$96 \times 128 \times 96$	2.7	16.2	3	IC2
11	$96 \times 128 \times 96$	2.7	16.2	3	IC2
12	$76 \times 128 \times 96$	2.1	16.2	3	IC2
13	$512 \times 1 \times 256$	3.4	0	1.7	IC2
14	$512 \times 1 \times 256$	3.4	0	1.7	IC2
15	$512 \times 1 \times 256$	3.4	0	1.7	IC1
16	$512 \times 1 \times 256$	1.7	0	1.7	IC1
17	$512 \times 12 \times 256$	1.7	0.12	0.8	IC3
18	$512 \times 1 \times 256$	1.7	0	1.7	IC3

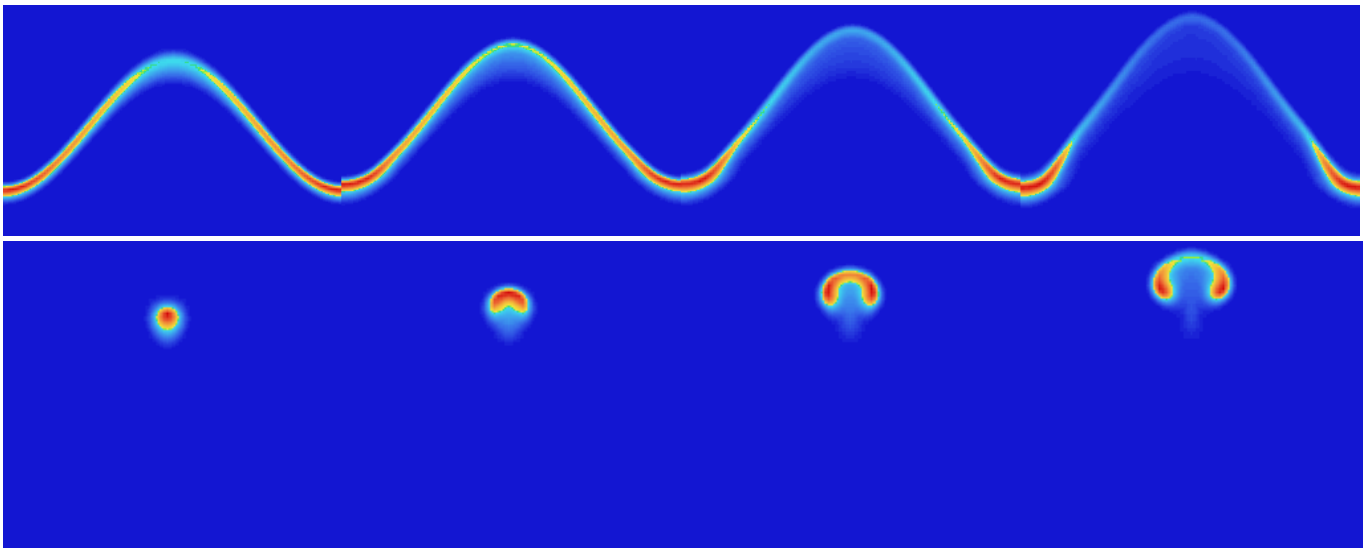

Fig. 1. A time evolution of the rising flux tube in four snapshots of E9. The upper panel shows B^2 in a slice through $z = 105$ Mm in the (y, x)-plane. The lower panel also shows B^2 but in a slice through $y = 600$ Mm — the (z, x)-plane through the apex

numerical resolution only postpones the inevitable; the thinning of the sheet proceeds exponentially. Since, the maximum of B/ρ remains on the line of symmetry for symmetric initial conditions that maximum is eventually lost in the thinning flux sheet. For the Gaussian initial conditions, the 'surviving' values of B/ρ in the spinning vortices are noticeably smaller than the initial maximum.

Schüssler (1979) found a similar behavior in a 2D numerical experiment of dimensions 60×20, assuming a constant field inside an initially cylindrical flux tube, and made the interesting remark concerning the (non-) analogy with a liquid drop: A flux tube is different from a liquid drop in that the drop has surface tension and the tube does not (because in the 2D geometry of Schüssler the tube has no magnetic tension along field lines). Schüssler therefore suggested that in a 3D scenario the fragmentation of the tube could possibly be prevented by magnetic tension, since the fragmentation of a liquid drop is prevented by its surface tension (for small drops). The 3D experiments that we have made show that this is indeed the case (cf. the discussion of experiment E17 below).

3.3. Evolution of a symmetric homogeneous flux tube

Fig. 3 illustrates the time evolution of experiment E16. This model has the IC1 initial magnetic field and therefore behaves as discussed in the previous subsection; the tube splits apart into fragments with small scale structure, resulting in a decrease of the buoyancy.

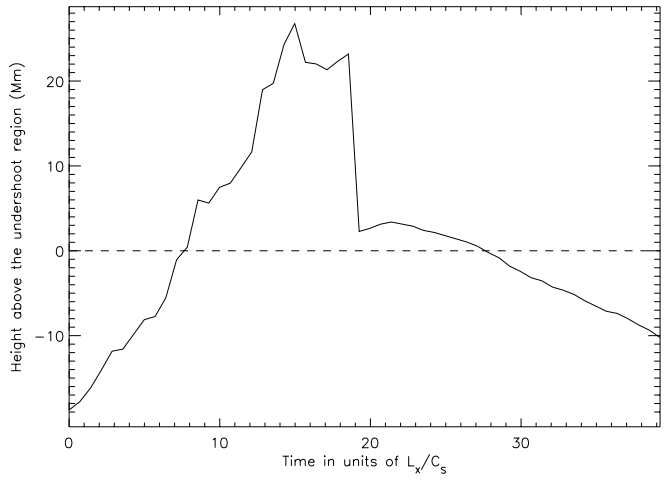

Fig. 2. The location of the point of maximum field strength is shown as a function of time, in units of $L_x/c_{\rm s}$ (from E16)

Because of the decrease of buoyancy, and because the spinning vortices are trapped in the exterior downdraft generated by the central ascent, most of the magnetic flux looses its ascent velocity. Fig. 2 shows the location of the point of maximum field strength as a function of time. After the initial increase of the vertical speed u_x resulting from the initial acceleration, a decrease of u_x follows that results from the loss of buoyancy. At around 19 times the sound crossing time τ_s ($\tau_s = L_x/c_S$) the magnetic field strength in the top part of the flux structure has dropped so much that the highest magnetic field strength now occurs in the rotating flux elements further down (cf. Fig. 3).

A remarkable picture emerges when this experiment is followed over many time steps. After the evolution through a mushroom shaped configuration with the creation of two oppositely rotating flux elements (snapshots 8-ff. in Fig. 3), some of the flux originally located in the center of the tube continues to rise. The front surface starts to develop ripples, because of a small scale R-T type instability. Suddenly a 'plume' is released (snapshots 18-20) from this rising flux element and descends down between the two counter rotating flux elements (snapshots 22-ff). At an even later stage the upper part of the flux structure has turned into a new mushroom shaped structure. The total range of time in Fig. 3 corresponds to $\sim 36\ \tau_s$. The two flux elements in the mushroom-structure keep rotating through the whole process and this helps them 'stay in shape'; they retain their identity and a significant magnetic flux, but their ascent is halted (and even reversed).

The behavior of E9 and E16 is a result of the fact that there is no mechanism that can hold the flux tube together. The flux tube looses its initial shape very quickly and the buoyancy vanishes, or is reduced so much that the flux fragments are easily caught by the downward drag of the external motion pattern set up by the initial ascent. The magnetic flux does not emerge at the surface within a foreseeable time. Hence these models cannot correspond to the buoyantly rising flux structures in the Sun that form the emerging flux regions, despite the fact that they are just more detailed versions of the otherwise successful 'thin flux tubes'. Mechanisms that can hold the flux together are clearly needed.

One can think of a several such mechanisms. The models show that when a flux tube splits into smaller structures these are born rotating. The rotation suppresses the R-T instability, and effectively holds the flux together into something that looks like a tube. Thus rotation is a possible stabilizing mechanism. Systematic rotation of the fragments that break loose from the toroidal flux system can probably be excluded, though; there is no plausible mechanism that would cause it.

One could argue that the initial splitting of a tube into two counter-rotating tubes might be enough, and that these two tubes would then be able to rise without further splitting (despite being caught in the downdrafts set up by the initial event). The end points of these tubes are anchored somewhere in the toroidal flux system, and hence the induced rotation will eventually be halted by the torsion built up along the tubes. The motion may be thought of as a reflected, torsional Alfvén wave). During the phase when motions are halted, the magnetic field has instead the maximum twist, and when the field lines straighten out, there is a maximum of the rotational motion.

The fragmentation process itself is thus to some extent able to create conditions that delay further fragmentation. However, tubes twisted more than a few turns end-to-end would become kink unstable, and the non-linear development of the kink would induce significant magnetic dissipation (cf. Galsgaard & Nordlund 1997). One might thus expect the initial angular momentum that caused the twist to be lost in the process. All-in-all it seems somewhat far fetched that these dynamic processes alone could be responsible for the seemingly coherent rise of buoyant flux tubes through the convection zone. It is thus of significant interest to consider flux tubes with more stationary stabilizing mechanisms "built-in".

Numerical simulations of dynamo processes indicate that the generated magnetic field may be very irregular, as the result of a chaotic mapping of field lines. It is thus natural to assume that the flux fragments breaking loose from the toroidal flux system has a significant amount of internal structure. The corresponding magnetic topology is likely to be non-trivial; i.e., the field lines are intertwined and cannot be moved apart without breaking the topology. In such a situation, one might expect there to be some built-in coherence to the flux tube; the topological constraint prevents the flux tube from breaking apart too easily. If such a mechanism can hold the flux together during most of its buoyant rise, this may solve the problem; the disruption/splitting is postponed until the tube is much closer to the photosphere.

3.4. Evolution of a 'chaotic' flux structure

Experiment E17 is an attempt to model chaos *along* field lines, in the spirit of the previous discussion. The initial field is quite arbitrary (but not current-free). It is constructed only with the objective to make its topology complex. The field is initially not in mechanical equilibrium; there are tension forces and pressure forces associated with the fluctuations. It should be noted that

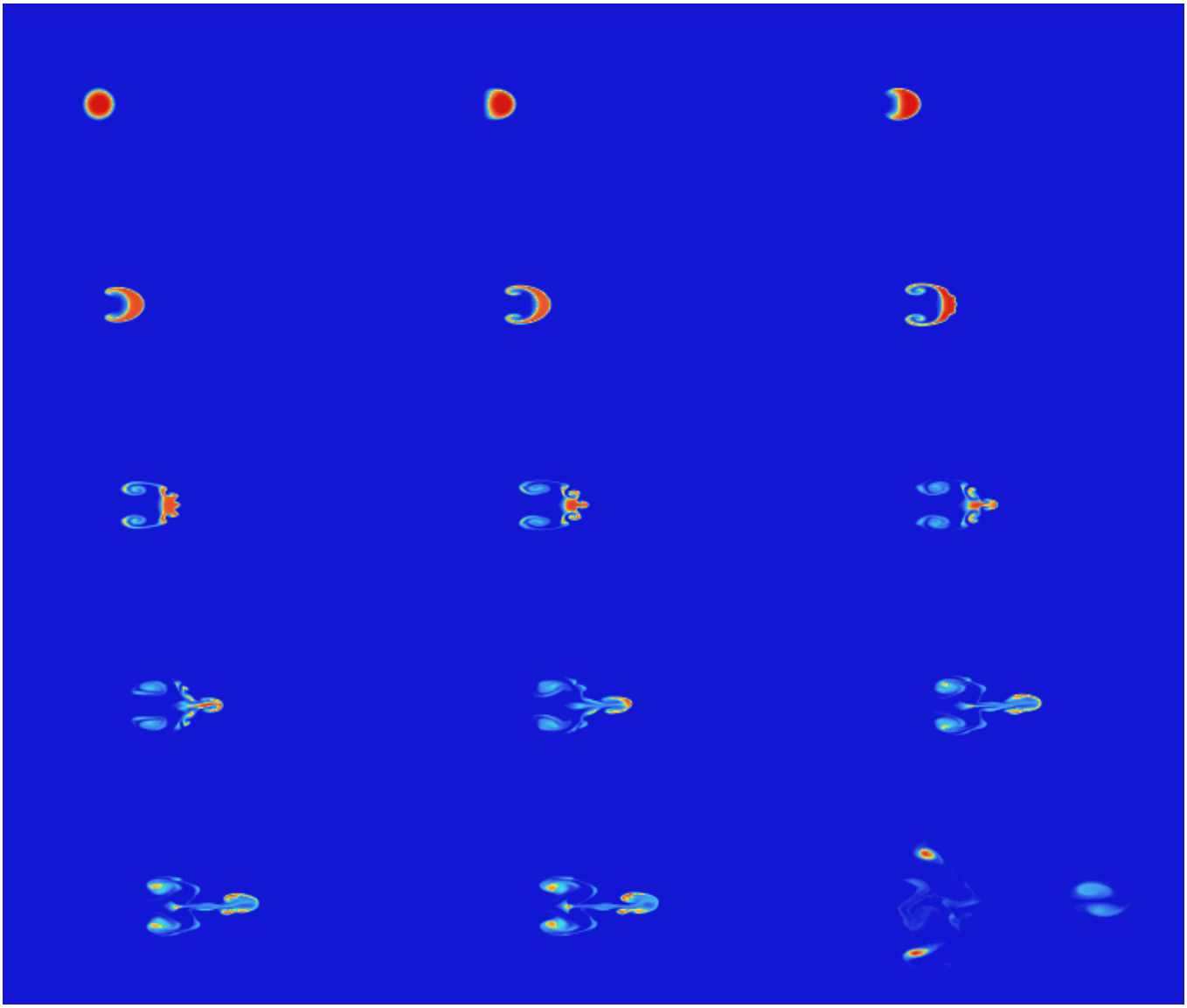

Fig. 3. Snapshots of B^2 in the plane (x, z) from E16: Snapshots (from left to right) 0, 2, 4, 6, 8, 10, 12, 14, 16, 18, 20, 22, 23, 24 and 51 (with 500 time steps between each snapshot).

according to the magnetostatic theorem of Parker (1975), such a system can never be in complete mechanical equilibrium. One may expect, though, that after some initial transients the evolution will slow down, and continue on a much longer, resistive time scale.

This is indeed what happens: Initially some transient processes occur, as a result of wave propagation along the field lines caused by magnetic tension forces. The basic effect of the transient is to 'untwist' the strong field component of the magnetic field in the flux tube so that it points almost completely in the y-direction, i.e. B_x and B_z become small for the highest values of B; after the transient the maximum values of B_x and B_y is typically about 10 % of the maximum of B_y. Only the weak field lines in the outer parts of tube can maintain their curvature, because the tension is too weak to 'untwist' them. This does not mean that the structure of the flux tube is now similar to that of the flux tube in e.g. E16; the field strength in the tube still has a randomly fluctuating weak field component. All through the ascent, the strong field is *not* unidirectional — even though the extent of the y-dimension is small in E17, the strong field shows small but non-zero B_x and B_z, a weak poloidal field is also present on the 'surface' of the flux tube throughout the experiment.

Because the transient takes place very fast, one might as well choose to view the state of the magnetic flux tube just after the transient as the initial condition. Fig. 4 shows the overall evolution of the toroidal magnetic field in experiment E17. After the transient and the initial buoyant acceleration the magnetic field continues to ascend with a nearly steady pace, with almost the entire flux contained within a small closed structure.

In the early stages the tube is predominantly held together by the chaotic mix of field lines within the tube, and the tension

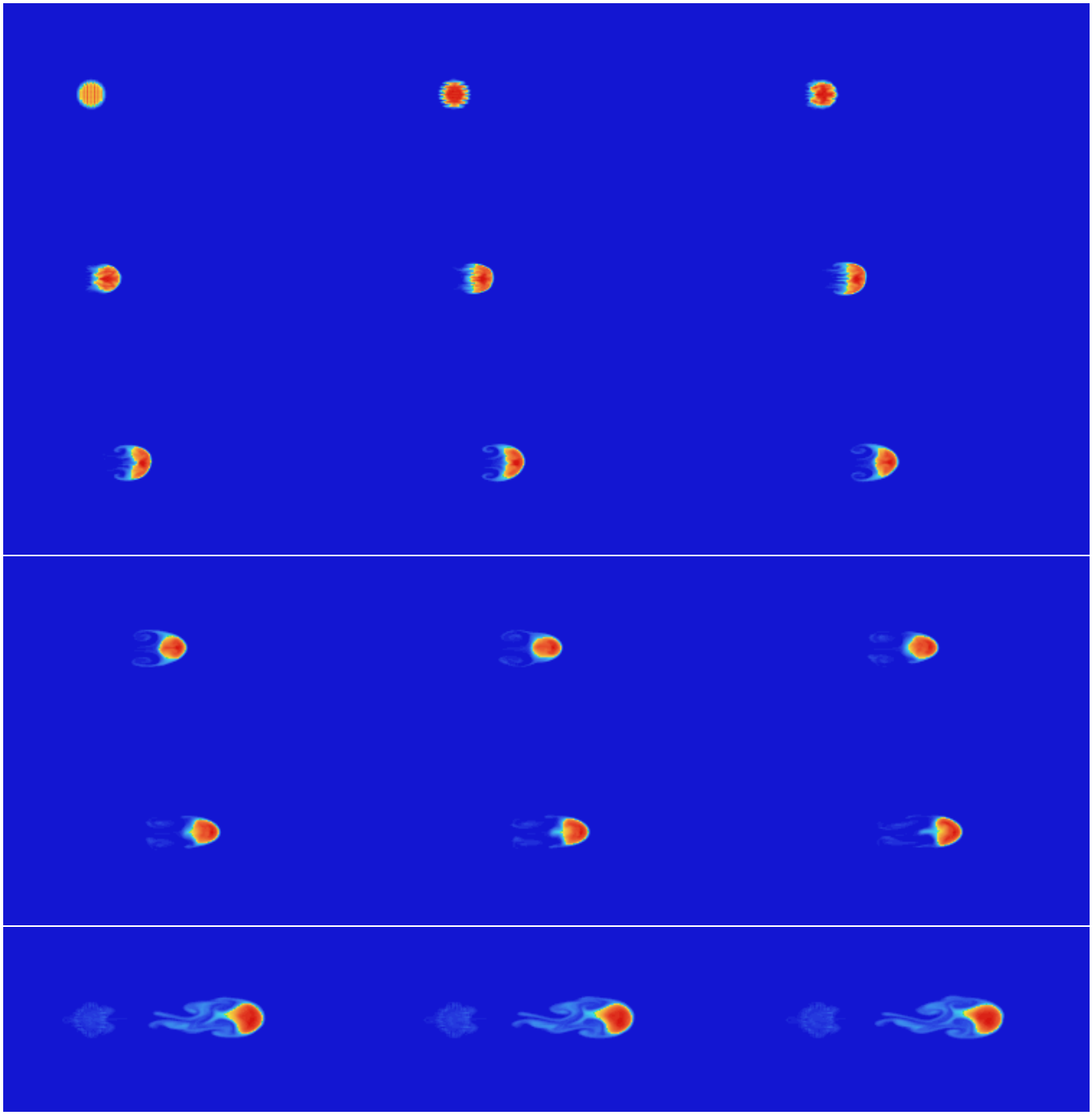

Fig. 4. Snapshots of B^2 in an (x, z)-plane from E17: Snapshots (from left to right) 0, 2, 4, 6, 8, 10, 12, 14, 16, 18 20, 22, 23, 24, 25, 30, 31 and 32

along the field lines. A mushroom-structure attempts to develop by the same processes that created it in the case of the initially homogeneous flux tubes, but in the present case these processes are suppressed. The 'surface' of the rising flux tube is what holds it together in the late stages; a 'core' of predominantly toroidal field lines is surrounded by a thin layer of weaker and predominantly poloidal magnetic field lines. The peak energy density of the poloidal surface field is about two orders of magnitude smaller than that of the toroidal field in the core, yet it is able to suppress the R-T type instability and hold the flux tube together.

In contrast to the case of the flux structure in E16, the ascent of the flux tube in E17 is much more well defined (cf. Figs. 2 and 5). In E16 the flux structure breaks into smaller fragments that spread all over the volume, making it hard to define at what

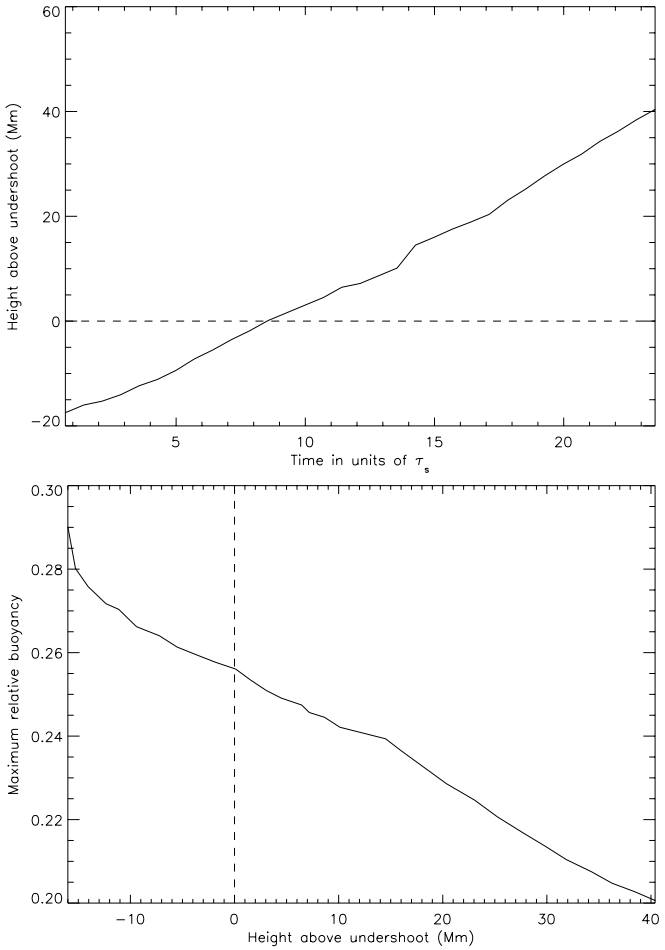

Fig. 5. The height of the point of maximum field strength versus time (upper panel), and the maximum relative buoyancy as a function of height (lower panel)

height 'the flux is located'. In E17 the flux stays localized and thus the ascent of the flux structure is well defined (cf. Fig. 5).

In the case of a flux tube ascending adiabatically with a polytropic stratification inside, the pressure varies as

$$P = P_0 \left(\frac{T}{T_0}\right)^{\gamma/(\gamma-1)} = P_0 \left(1 - \frac{\gamma-1}{\gamma}\frac{(x-x_0)}{H_0}\right)^{\gamma/(\gamma-1)}, \quad (11)$$

where T is the temperature, H is the pressure scale height and the index 0 refers to the height where the flux tube begins the ascent. Since B/ρ must be constant, this implies that the magnetic field of such a flux tube decreases with height as

$$B(x) = B_0 \left(1 - \frac{\gamma-1}{\gamma}\frac{(x-x_0)}{H_0}\right)^{1/(\gamma-1)}. \quad (12)$$

A comparison between the Eq. 12 and experiment E17 is shown in Fig. 6.

The maximum magnetic field strength of the flux tube in model E17 is indeed well described by Eq. 12; this shows that

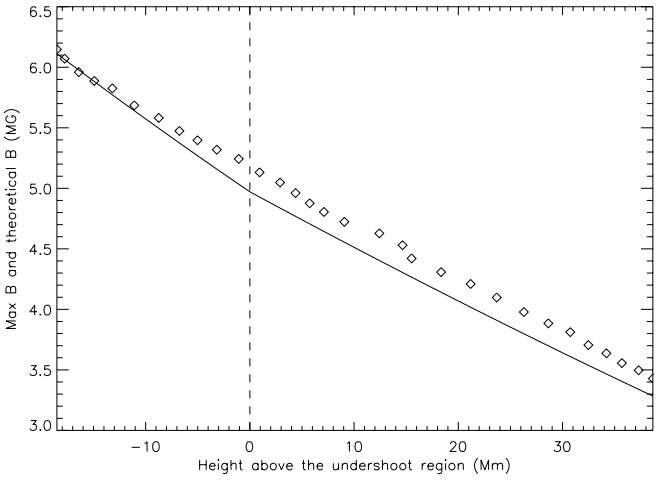

Fig. 6. The decrease with height of an adiabatic flux tube ($\gamma = 5/3$) with a polytropic stratification obeying $B/\rho =$ constant (solid line), compared with the decrease of the maximum field strength of the flux tube in E17

the reason for the decrease of the magnetic field strength is the ascent into layers with decreasing pressure, and that other field weakening processes have little effect.

In the early stages of the buoyant rise, a structure develops that looks a bit like the mushroom-structure discussed in the case of E16. In this case it is, however, located in the 'wake' of the flux tube, and has a very small field strength. The mushroom-structure formation is a side effect, caused by the external velocity field that is able to rip-off some of the weak field lines from the 'surface' of the tube and mix these into the plasma in the wake. Eventually, the wake structure undergoes a transition and becomes chaotic (cf. Fig. 4).

Apart from keeping a tube-like structure and a relatively high value of buoyancy, the flux structure in E17 also has another interesting property. Even though most of the flux is transported upwards in the box, the ripping-off of the surface layer means that the structure 'leaks' a weak field into the ambient medium.

The field strength in the 'wake' of the flux structure attains typical values of only 0.1-1 % of the peak value of the field. The fate of this weak field, which has practically no buoyancy and becomes mixed into the ambient plasma, depends on the local velocity field topology.

We do not model the convective velocity field explicitly in our model, but the topological properties of convection in a stratified medium are known from other experiments (Stein & Nordlund 1998). By following test particle motions, Spruit et al. (1990) showed that the average depth of a set of test particles always increases with time if the particles are followed for a sufficiently long time. Even a subset of particles that are all initially ascending soon turn over and become, on the average, descending. This property is a direct consequence of mass conservation; most of the ascending fluid at any one height must turn over within one density scale height, in order to not change the average stratification. As demonstrated by more recent experiments with higher numerical resolution

($253^2 \times 163$; Stein & Nordlund 1998), this property is robust and does not depend on whether the flow is laminar or turbulent.

We thus expect that the fate of sufficiently weak magnetic fields in the real solar convection zone, such as the 'wake' fields found in the present experiments, is to be pulled down by the stratified convection. This may be an interesting mechanism for replenishing the dynamo magnetic field at the bottom of the convection zone.

4. Summary and discussion

From the above discussions and experiments with various initial conditions, it may be seen that there are at least three different mechanisms that tend to disrupt buoyantly ascending flux tubes:

1. the R-T like instability that is effective even in the limit of a very 'thin flux tube' and disrupts the tube by creating a mushroom-like flux structure,
2. the expansion of the tube and the decrease of the pressure scale height, that will tend to fragment the flux tube to prevent the size from becoming much larger than the scale height,
3. the explosion of a tube in hydrostatic equilibrium in a superadiabatic convection zone (cf. Moreno-Insertis et al. 1995).

Which of these mechanisms that comes into operation first depends strongly on the initial conditions for the ascending flux tube; a topologically simple flux tube is rapidly destroyed by the R-T like instability, while a flux tube with a complex topology but a too small total magnetic flux (and hence a sufficiently slow ascent to maintain approximate pressure equilibrium along the field lines) may 'explode' before it reaches the surface layers (cf. Moreno-Insertis et al. 1995). Flux tubes with both a complex topology, and with a sufficient magnetic flux to ascend rapidly, may be expected to survive the longest, but eventually these must also break up into thinner fragments, in order to ascend all the way to the surface where the vertical scale height is very small.

The $\sim 10^5$ Gauss fields at the bottom of the convection zone that have been shown to give consistent tilt angles and emergence latitudes (D'Silva & Choudhuri 1993; Fan et al. 1993; Fan et al. 1994; Caligari et al. 1995) can only do so if their buoyant rise is reasonably well described by the thin flux tube approximation. In particular, the speed of ascent is determined by a balance between buoyancy and drag (and magnetic tension), and is derived assuming circular cross sections. If the cross sections become distorted but the structure remains intact, the speed of ascent will be approximately the same as for a circular cross section (for a flattened structure the increased drag will make it somewhat smaller), but if it breaks up into many fragments, the drag will increase in proportion to the number of fragments. Note that alternative models have been proposed, where giant cell flows and exchange of longitudinal momentum between the flux tube and its surroundings is invoked to produce the proper emergence patterns and tilt angles even for fragmented flux tubes (Choudhuri & D'Silva 1990; D'Silva & Choudhuri 1991; Choudhuri 1992; D'Silva 1993).

The requirement that the magnetic field in the buoyantly ascending magnetic flux structures should have a non-trivial topology may be considered as a reminder about the presumably chaotic nature of the toroidal flux system at the bottom of the solar convection zone. The power laws that describe the size distribution of the emerging flux regions (Schrijver & Harvey 1994) may indicate a selfsimilar and perhaps fractal structure of the toroidal flux system. We thus envisage that a cross section of the toroidal flux system would reveal an intermittent distribution of fragments of various sizes, where each fragment also has a non-trivial internal topology.

Numerical simulations of a magnetic field embedded in a turbulent medium (Nordlund et al. 1994) indeed illustrate how cross-field convergence and divergence of the velocity field is able to shape a distribution of magnetic field concentrations. Each concentration is coherent along the magnetic field direction, but only for a limited distance. Over longer distances, the magnetic field lines wander between individual flux concentrations that, given the appearance in 3D isosurface renderings perhaps should be called 'flux cigars', rather than 'flux tubes'.

With the differential rotation that is present at the bottom of the solar convection zone, such a flux structure would be continuously stretched out in the longitudinal direction, much as the toroidal magnetic field in numerical simulations of accretion disks (Brandenburg et al. 1995). As the magnetic field strength increases because of the stretching, individual cross sectional fragments will become buoyantly unstable and start to ascend.

In such a scenario it is natural to assume that the fragments that break loose and start to ascend already has a chaotic internal field line topology and some overall twist. They would thus, according to the present investigation, be 'immunized' against R-T like instabilities.

5. Conclusions

By conducting the numerical experiments summarized in Table 1, corresponding to different models of buoyantly rising flux tubes in the Sun, we have obtained the following results:

- If the magnetic field lines of the initial flux tube are entirely parallel (either with a constant field strength across the flux tube cross section or with a peak at the center) the flux tube is quickly disrupted by a R-T like instability.
- If the initial flux tube has a non-trivial topology, the flux structure is held together for a longer time and is able to keep most of its buoyancy.
- A weak field that eventually is mixed into the ambient medium is shredded into the wake of the rising flux structure.

The main conceptual conclusion of this work is that the topology of the magnetic field in buoyantly ascending magnetic flux structures has a profound effect on their behavior. One might say that, in order for the 'thin flux tube approximation' to be valid, the magnetic field must not be in the form of 'thin flux

tubes' with exatly parallel field lines. Rather they should be in the form of 'thin flux ropes', i.e., there must be some internal structure that makes the topology non-trivial, in order to prevent buoyant magnetic fields from breaking apart.

Future work should address both the initial conditions for the buoyantly rising flux structures, and their subsequent fate in layers close to the solar surface in more detail than has been discussed here. The possibility of 'explosions' (Moreno-Insertis et al. 1995) or 'dynamic disconnection' (Fan et al. 1994) of the magnetic flux structures beneath the solar surface should be investigated.

An immediate extension of the current work would be to continue the simulations into layers closer to the surface, where the scale heights are much smaller than the typical size of the ascending flux structures. This requires a large number of 3D grid points, since the vertical direction must encompass several well resolved scale heights, and the resolution in the two horizontal directions should be comparable to the one in the vertical direction. The horizontal scale should be of the order of 10 – 100 Mm, to cover the size of typical emerging flux regions. Such a simulation would probably benefit from a possibility to rezone the simulation at regular intervals, to follow the flux structure as it ascends, and rescale the mesh resolution as dictated by the local scale heights.

Simulations are currently being made to study the evolution of an initially horizontal field at the very surface, on the scale of the solar granulation (Bercik et al. 1997; Stein et al. 1998). On this scale, one is essentially studying the small scale structure of one of the fragments of an emerging flux regions. On the basis of these simulations one will be able to better understand the complicated interaction between the magnetic field and the radiation-influenced convection in the surface boundary layer, and make predictions about observable quantities,

Acknowledgements. This work was supported in part by the Danish Research Foundation, through its establishment of the Theoretical Astrophysics Center. Computing time on the CM-200 at the UNI•C computing center was provided by the Danish Natural Science Research Council

References

Babcock, H. 1961, ApJ, 133, 572
Bercik, D. J., Basu, S., Georgobiani, D., Nordlund, Å., Stein, R. F. 1997, in Stellar Systems and the Sun, Astronomical Society of the Pacific Conference Series
Brandenburg, A., Nordlund, A., Stein, R. F., Torkelsson, U. 1995, Astrophys. J., 446, 741
Caligari, P., Moreno-Insertis, F., Schussler, M. 1995, ApJ, 441, 886
Cattaneo, F., Chiueh, T., Hughes, D. 1990, J. Fluid Mech., 219, 1
Cattaneo, F., Hughes, D. 1988, J. Fluid Mech., 196, 323
Choudhuri, A. 1992, in J. Thomas, N. Weiss (eds.), Sunspots: Theory and Observations, Kluwer, p. 243
Choudhuri, A., D'Silva, S. 1990, A&A, 236, 326
Choudhuri, A. R. 1989, Solar Phys., 123, 217
Choudhuri, A. R., Gilman, P. 1987, ApJ, 316, 788, first paper to argue for 10^5 Gauss?
D'Silva, S. 1993, ApJ, 407, 385
D'Silva, S., Choudhuri, A. 1991, Solar Phys., 136, 201
D'Silva, S., Choudhuri, A. 1993, ApJ, 272, 621
Emonet, T., Moreno-Insertis, F. 1996a, ApJ, 458, 783
Emonet, T., Moreno-Insertis, F. 1996b, ApJ, 472, L53
Emonet, T., Moreno-Insertis, F. 1997, in Advances in Physics of Sunspots, Vol. 118, 71
Emonet, T., Moreno-Insertis, F. 1998, ApJ, 492, 804
Fan, Y., Fisher, G., DeLuca, E. 1993, ApJ, 405, 390
Fan, Y., Fisher, G., McClymont, A. 1994, ApJ, 436, 907
Gaizauskas, V. 1993, Adv.Space Res., 13, (9)5
Galsgaard, K., Nordlund, Å. 1997, Journal of Geophysical Research, 102, 219
Hyman, J. 1979, in R. Vichnevetsky, R. S. Stepleman (eds.), Adv. in Comp. Meth. for PDE's—III, 313
Leighton, R. 1964, ApJ, 140, 1547
Leighton, R. 1969, ApJ, 156, 1
Longcope, D., Fisher, G. 1996, ApJ, 464, 999
Longcope, D., Fisher, G., Arendt, S. 1996, ApJ, 464, 999
Matthews, P., Hughes, D., Proctor, M. 1995, ApJ, 448, 938
Moreno-Insertis, F. 1986, A&A, 166, 291
Moreno-Insertis, F. 1997, in Advances in the Physics of Sunspots, Vol. 118, p. 45
Moreno-Insertis, F., Caligari, P., Schussler, M. 1995, ApJ, 452, 894
Moreno-Insertis, F., Schussler, M., Ferriz-Mas, A. 1992, A&A, 264, 686
Nordlund, A., Galsgaard, K. 1997, Journal of Computational Physics, (in preparation)
Nordlund, A., Galsgaard, K., Stein, R. F. 1994, in R. J. Rutten, C. J. Schrijver (eds.), Solar Surface Magnetic Fields, Vol. 433, NATO ASI Series
Parker, E. N. 1955, apj, 121, 491
Parker, E. N. 1975, ApJ, 201, 494
Schrijver, C., Harvey, K. 1994, Solar Phys., 150, 1
Schüssler, M. 1979, A&A, 71, 79
Sheeley, N. R. 1992, in The Solar Cycle, Vol. 27 of *Astron. Soc. of the Pacific Conf. Series*, p. 1
Spruit, H. 1974, Solar Phys., 34, 277
Spruit, H. 1981, A&A, 98, 155
Spruit, H., Nordlund, Å., Title, A. 1990, ARA&A, 28, 263
Stein, R. F., Bercik, D. J., Georgobiani, D., Nordlund, A. 1998, ApJ, (in preparation)
Stein, R. F., Nordlund, A. 1998, Astrophys. J., 499, 914
Tsinganos, K. 1980, ApJ, 239, 746
Wang, H., Zirin, H., Ai, G. 1991, Solar Phys.
Wang, Y.-M., Sheeley, N. R. 1991, ApJ, 375, 761